Disentangling Electron-phonon Coupling and Thermal Expansion Effects in the Bandgap Renormalization of Perovskite Nanocrystals

Andrea Rubino[1], Adrián Francisco-López[2], Alex Barker[3], Annamaria Petrozza[3], Mauricio E. Calvo[1], Alejandro R. Goñi[2,4,], Hernán Míguez[1,*]*

[1]Institute of Materials Science of Seville, Spanish National Research Council-University of Seville, C/Américo Vespucio 49, 41092, Seville, Spain.

[2]Institut de Ciència de Materials de Barcelona, ICMAB-CSIC, Campus UAB, 08193 Bellaterra, Spain.

[3]Instituto Italiano di Tecnologia, CNST, Milano.

[4]ICREA, Passeig Lluís Companys 23, 08010 Barcelona, Spain.

*corresponding authors: h.miguez@csic.es; goni@icmab.es

ABSTRACT. The complex electron-phonon interaction occurring in bulk lead halide perovskites gives rise to anomalous temperature dependences, like the widening of the electronic bandgap as temperature increases. However, possible confinement effects on the electron-phonon coupling in the nanocrystaline version of these materials remain unexplored. Herein we study the temperature (ranging from 80 K to ambient) and hydrostatic pressure (from atmospheric to 0.6 GPa) dependence of the photoluminescence of ligand-free methylammonium lead triiodide nanocrystals with controlled sizes embedded in a porous silica matrix. This analysis allowed us to disentangle the effects of thermal expansion and electron-phonon interaction. As the crystallite size decreases, the electron-phonon contribution to the gap renormalization gains in importance. We provide a plausible explanation for this observation in terms of quantum confinement effects, showing that neither thermal expansion nor electron-phonon coupling effects may be disregarded when analyzing the temperature dependence of the optoelectronic properties of perovskite lead halide nanocrystals.

Graphic for TOC

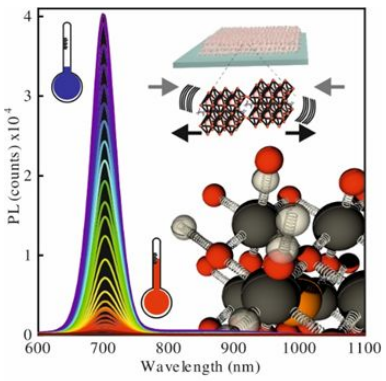

Nanostructured metal halide perovskites show great potential for next-generation light sources,[1,2] allowing precise control of their optoelectronic properties through the discretization of the electronic energy spectrum and the concomitant changes in the density of states.[3] The pioneering work of Pérez-Prieto *et al.*[4] and Kovalenko *et al.*[5] on metal halide perovskites of the type ABX_3, where A is a monovalent inorganic or organic cation (e.g., methylammonium (MA), formamidinium (FA), cesium Cs), B is a metal cation (Pb, Sn) and X is a halide anion (Cl, Br, I), contributed to the development of lead halide colloidal nanocrystals which exhibited high photoluminescence (PL) quantum yields and a band-gap tunable in a broad spectral range.[6] Most of the literature on perovskite nanocrystals (NCs) concern the study of the PL emission properties, partly as a function of temperature or pressure, using continuous wave and/or pulsed excitation in order to determine key radiative recombination parameters in different nanocrystalline materials such as $MAPbI_3$,[7-9] $MAPbBr_3$,[10-13] $FAPbI_3$,[9,14,15] $FAPbBr_3$,[7,13,16,17] $CsPbI_3$,[5,7,18-20] $CsPbBr_3$,[5,7,13,18,19,21-24] and $CsPbCl_3$.[5,7,18]

For many optoelectronic applications, precise knowledge about the semiconductor band-gap and its dependence on temperature is mandatory. In principle, the effect of a temperature change on the electronic band structure is twofold. On the one hand, the electronic band states move in energy upon changes in the lattice potential due to the temperature-induced contraction/expansion of the lattice. On the other hand, lattice vibrations also affect the effective potential leading to an energy renormalization of the electronic band structure, which is generally stronger for higher temperatures. Hence, the derivative of the gap over temperature contains two terms, accounting for thermal expansion (TE) and electron-phonon (EP) interaction effects:[25-27]

$$\frac{dE_g}{dT} = \left[\frac{\partial E_g}{\partial T}\right]_{TE} + \left[\frac{\partial E_g}{\partial T}\right]_{EP} \qquad (1)$$

TE usually adopts negative values whereas EP could be positive or negative. However, for most conventional semiconductors both TE and EP terms are negative, causing a reduction of the gap with increasing temperature.[25,27,28] On the contrary, the structural phases of lead halide perovskites that are stable at ambient conditions exhibit the opposite behavior: the gap increases linearly with increasing temperature.[29-37]

Regarding the temperature dependence of the bandgap of perovskite NCs, there is evidence that indicates that it differs significantly from that of their bulk counterparts.[9,14,16,21] In perovskite colloids,[5,6] it is rather difficult to discern the contribution from the solvent, but above all from the ligands, particularly when identifying certain crystalline lattice vibrations. Sometimes, a pronounced bowing and/or a non-monotonous temperature dependence is observed,[18,20] which cannot be clearly associated with changes occurring in the crystalline structure, because there is no obvious match with the transition temperatures of the bulk.[8,9] Strikingly, a well-defined gap bowing spanning a wide temperature range in excess of 150 K has been systematically observed for a whole series of $FA_xMA_{1-x}PbI_3$ solid-solution single crystals.[37] The temperature dependence of the gap in certain perovskite NCs thus resembles this behavior. The question that arises is what is the cause for such phenomenology and if a peculiarly strong electron-phonon interaction is at its origin, as it has been suggested.[11,15,16,18]

In this work, we have combined PL experiments as a function of temperature and pressure, at ambient pressure and at room temperature, respectively, in order to analyze the importance of thermal expansion and electron-phonon coupling effects on the temperature-induced gap renormalization in $MAPbI_3$ nanocrystals of different size. The nanocrystals were prepared through a template-assisted method that leads to ligand-free perovskite NCs, embedded in a high optical quality SiO_2 matrix film, which exhibit bright light emission properties.[10] An indisputable advantage of this method is the absence of solvent residues and any kind of ligands that can compromise the optoelectronic properties of the perovskite nanostructures or, central to the study herein presented, modify their intrinsic temperature and pressure dependence. In addition, the rather large band gap of the surrounding silica ensures optimal quantum confinement of electrons and holes in the NCs. A primary result of this work concerns the enhancement of the electron-phonon interaction contribution to the gap renormalization observed at room temperature for $MAPbI_3$ NCs with decreasing size.

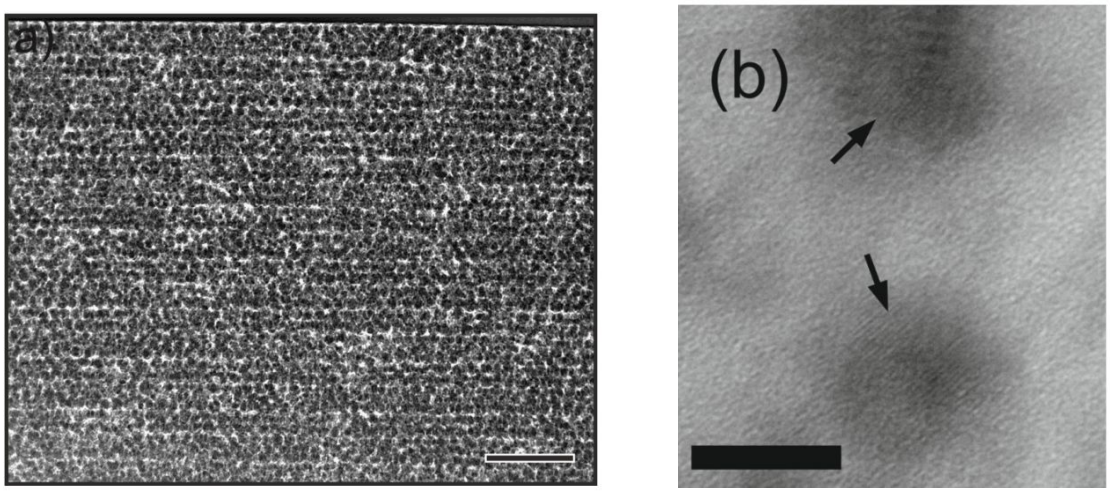

Figure 1: (a) High-angle annular dark-field scanning TEM image of a cross section of a SiO_2 nanoparticles mesoporous film corresponding to a $MAPbI_3$ NC sample with average diameter of 8 nm. Scale bar is 200 nm. (b) High-resolution TEM image of the same $MAPbI_3$ nanocrystals shown in part (a). Scale bar is 10 nm.

Optical quality (i.e., scattering free) films of porous silica hosting $MAPbI_3$ nanocrystals of well-defined average diameter were obtained following a procedure described in detail elsewhere.[10] In Fig. 1a we show an image of a cross section of a representative porous SiO_2 film containing c.a. 8 nm size $MAPbI_3$ NCs, attained in high-angle annular dark-field scanning mode. Brighter regions indicate the position of perovskite NCs (heavier atoms). Fig. 1b displays a high magnification transmission electron microscopy (TEM) image in which the positions of perovskite nanocrystals (darker spots) are indicated by arrows. More information about the specific conditions herein employed, the EDX analysis, particle size distribution, and temperature dependence of X-ray diffraction (XRD) and Raman spectroscopy are provided as Supplementary Information (SI, see Figs. S1-S8).

The normalized PL spectra recorded at room temperature for both the $MAPbI_3$ thin film and nanocrystals of different sizes (namely, 8 nm, 5 nm and 4 nm in diameter) are shown in Fig. 2a. The PL spectra consists essentially of a single broad peak, assigned to free-exciton radiative recombination.[37,38] This assignment is explained in detail and justified in the SI, under the title "On the excitonic character of the PL emission". Analysis of peak spectral position using Brus formula[39] yielded average nanocrystal values similar to those attained from the TEM image

analysis, which we will use hereafter to tag the different samples studied in this work. Figs. 2b to 2e display, through color maps, the PL change as a function of temperature in the range from 80 K to 300 K, for a bulk $MAPbI_3$ thin film and three composite samples with nanocrystals of different sizes, namely 8 nm, 5 nm and 4 nm. We also show, in Figs. S9 and S10 the PL spectra recorded for each sample, as well as representative examples of the PL line shape fits attained by using a Gaussian−Lorentzian cross-product function.[37,38] Interestingly, the non-monotonic temperature behavior exhibited by the peak position of the free-exciton PL is different for each nanocrystal size considered. Changes in the tendency of the maximum peak energy might be related to the occurrence of different phase transitions in the temperature range of the experiment. Furthermore, the low-temperature emission spectra of the $MAPbI_3$ thin-film sample display a broad peak below 120 K at longer wavelengths than 800 nm (<1.55 eV) (see Fig. 2b). At very low temperatures, the photo-excited carriers can readily form exciton complexes bound to shallow impurities (acceptors and/or donors) present in an unintentionally-doped semiconductors.[3] Hence, the peak below the free-exciton peak observed at low temperatures could be ascribed to radiative recombination of bound-exciton complexes, as reported elsewhere.[11,19,37] For the NC samples, however, only the free-exciton peak is observable in the whole temperature range of the experiments, possibly indicating that the synthetic procedure employed yields almost defect-free nanocrystals.[10] Another conclusion that can be drawn from the results of Figs. 2b-2e is that only the thin film sample seems to show a sudden change in the temperature dependence of the PL peak energy at around 150 K, which can be associated with the occurrence of the tetragonal-to-orthorhombic phase transition.[40] In fact, below 150 K the PL spectra of the thin-film sample display two peaks closely located at ca. 750 nm, which speaks for the coexistence of both the orthorhombic and the tetragonal phases of $MAPbI_3$.[8,37] In contrast, for the NC samples the temperature dependence of the PL peak energy is always smooth, though less pronounced for decreasing NC size. Similar absence of any sign of this phase transition has been previously observed for small $MAPbI_3$[8] and $MAPbBr_3$[20] NCs.

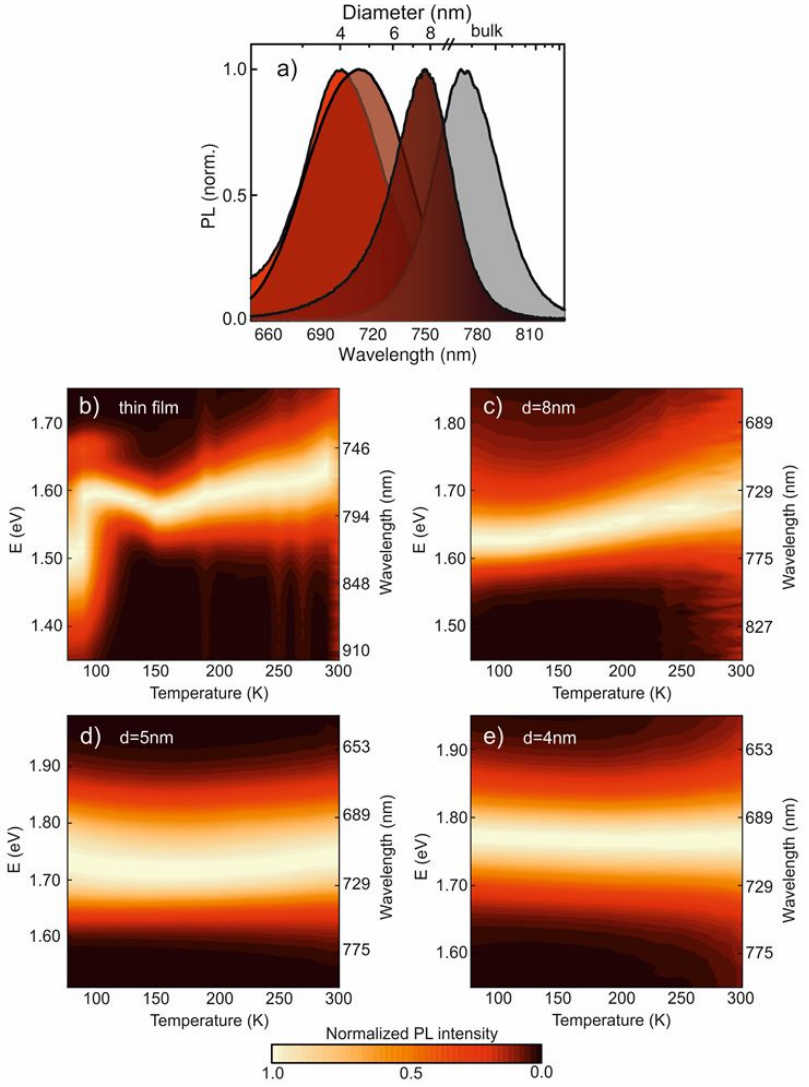

Figure 2. (a) Room-temperature normalized PL spectra of the different nanostructured $MAPbI_3$ samples corresponding to a polycrystalline thin film (grey-filled spectrum) and NCs of estimated average diameter of 8 nm, 5 nm, and 4 nm(red-filled curves). (b-e) Color maps of normalized PL spectra recorded at different temperatures from 80 K to 300 K for (b) thin film and the NCs embedded in a silica matrix corresponding to average NC sizes of (c) 8 nm, (d) 5 nm, and (e) 4 nm.

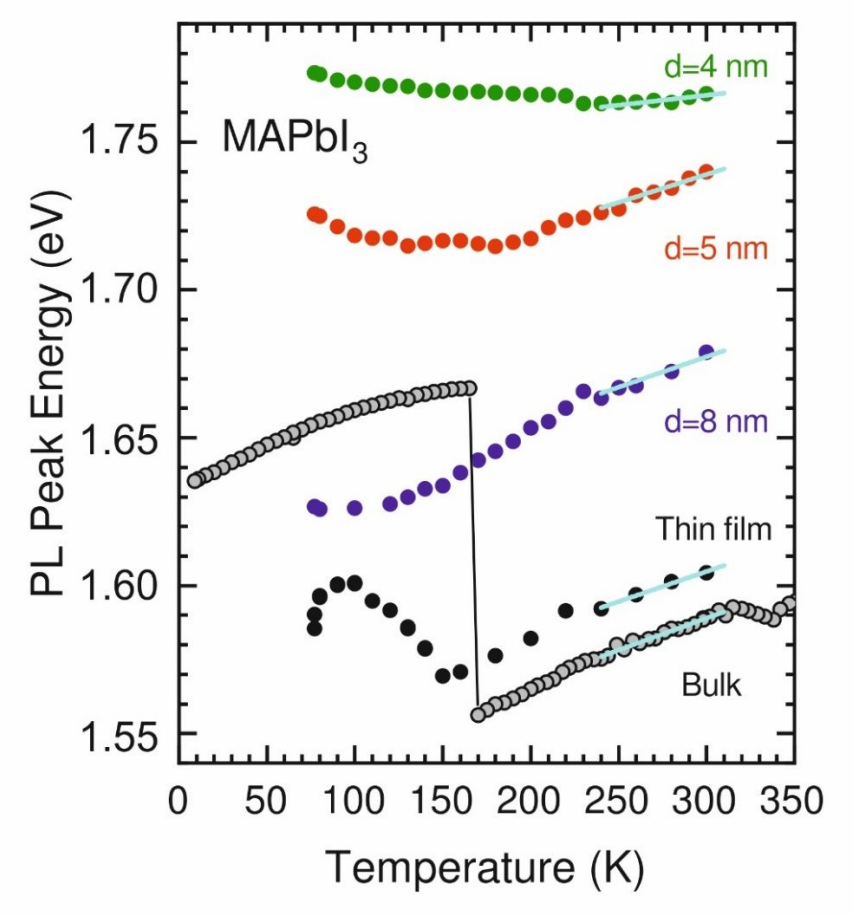

Figure 3: Temperature dependence of PL peak maximum position (close symbols) for different $MAPbI_3$ samples, corresponding to a single crystal (denoted as bulk), a thin film and nanocrystals with different average diameters d, as indicated. Cyan lines represent the linear regression fits to the data points solely in the temperature range between 240 K and 300 K.

The values of the fitting parameter corresponding to the peak energy are plotted as a function of temperature in Fig. 3 for three NC samples (blue, red and green symbols) and a polycrystalline thin film (black solid symbols), together with data obtained for a high-quality $MAPbI_3$ single crystal, denoted as bulk (grey symbols). Since the exciton binding energy in $MAPbI_3$ is relatively small (ca. 15 meV),[41,42] we can consider the shift of the PL peak energy E_0 with temperature really representative of the temperature shift of the optical gap, such that we set $E_0=E_g$. As anticipated, the sudden jump in the gap energy at the tetragonal-to-orthorhombic phase transition, clearly apparent in the data of the single crystalline bulk,[37] is only observed as a kink in the E_g vs. T curve of the thin film. On the contrary, there are no signs of such first-order transformation for the NC samples. In turn, these samples exhibit a positive bowing that changes

in magnitude depending on NC size. For completeness, we show the fitted values of the FWHM and PL integrated intensity in Figs. S11 and S12, respectively, of the SI.

A careful inspection of the data displayed in Fig. 3 indicates the existence of common characteristics in the temperature behavior of E_g, shared by all studied samples. At around room temperature, in the stability range of the tetragonal phase of $MAPbI_3$ bulk, the gap decreases linearly with decreasing temperature. This behavior has been recently analyzed in $MAPbI_3$ and ascribed to a comparable effect of TE and EP renormalization.[34] For the NC samples this linear dependence holds at least down to a temperature of about 240 K. The unusual temperature dependence of the gap observed at temperatures below 240 K for the NC samples, which develops a more or less pronounced positive bowing depending on NC size, might be affected by phase transitions for which we lack an accurate description. Hence, we will restrict our analysis to T>240 K, although a brief discussion on potential effects that may be taking place in that range is included in the SI. The solid cyan lines in Fig. 3 represent the results of least-squares fits to the E_g vs T data points performed in the range from 240 K to 300 K. The corresponding slopes obtained from the fits are listed in Table I, including the results for the $MAPbI_3$ thin film and the single-crystal bulk sample. The slopes acquire a pretty constant value of ca. 0.21 meV/K, diminishing only for very small NC sizes.

Now, in order to estimate the contribution from thermal expansion effects to the temperature slope dE_g/dT (Eq. 1) in the tetragonal phase, we make use of the following relation:[25-27]

$$\left[\frac{\partial E_g}{\partial T}\right]_{TE} = -\alpha_V \cdot B_0 \cdot \frac{dE_g}{dP} \qquad (2)$$

where α_V is the volumetric thermal expansion coefficient, B_0 is the bulk modulus and dE_g/dP is the gap pressure coefficient, which can be experimentally determined by measuring the dependence of the PL with applied pressure.[38,43] For that purpose, we have performed hydrostatic pressure PL experiments at room temperature for several NC samples with different NC sizes, in order to assess the gap pressure coefficients dE_g/dP. In Fig. S13 we show the spectra recorded for two nanocrystal sizes (5 nm and 8 nm). Since these experiments are performed under isothermal conditions, the EP term remains unchanged when the variation of the gap with

pressure is measured. In our case, only the data collected up to a pressure of approx. 0.6 GPa are relevant, since at that value $MAPbI_3$ crystalline structure transforms from tetragonal to a cubic high pressure phase.[38,44] Like before, PL spectra measured under pressure were analyzed using a Gaussian-Lorentzian cross-product function. The resulting PL peak energies are plotted in Fig. 4a as a function of applied pressure. In total agreement with the results obtained for $MAPbI_3$ bulk (high-quality single crystals),[34,38] we also attain a negative linear dependence on pressure of E_g for the NC samples. The solid color curves in Fig. 4a represent least-squares fit to the data points using a linear function. Such a negative pressure dependence of E_g can be understood for the bulk perovskite in terms of the bonding/antibonding and the atomic-orbital character of the conduction and valence band states involved in the optical transition.[38] Incidentally, according to Eq. (2) a negative pressure coefficient implies a positive contribution from thermal expansion to the temperature slope dE_g/dT, which adds up to that from electron-phonon interaction effects.

A series of sacrificial samples with different nanocrystal sizes were prepared to measure the gap energy pressure coefficient. Results are shown in Fig. 4. The value of the gap energy at ambient conditions (T=300 K, P=1 bar), $E_{g,300K}$, should steadily increase with decreasing NC size.[39] We thus plot the measured pressure coefficients, corresponding to the slopes of the fitted lines to the data points of Fig. 4a, as a function of the gap energy at ambient pressure-temperature conditions $E_{g,300\ K}$ and obtain the graph depicted in Fig. 4b. The red curve is just a least-squares fit to the data points using an empirical quadratic function. This graph clearly shows that the absolute value of the linear pressure coefficient of the gap energy, $|dE_g/dP|$, decreases with decreasing NC size, i.e. the stronger the quantum confinement effects are. A similar behavior has been already observed in a variety of systems like Si NCs[45] and amorphous Si nanoparticles[46] both embedded in a SiO_2 matrix, or colloidal CdTe[47] and $CsPbBr_3$[24] NCs, which indicates that it might be a general trend in zero-dimensional semiconductors.

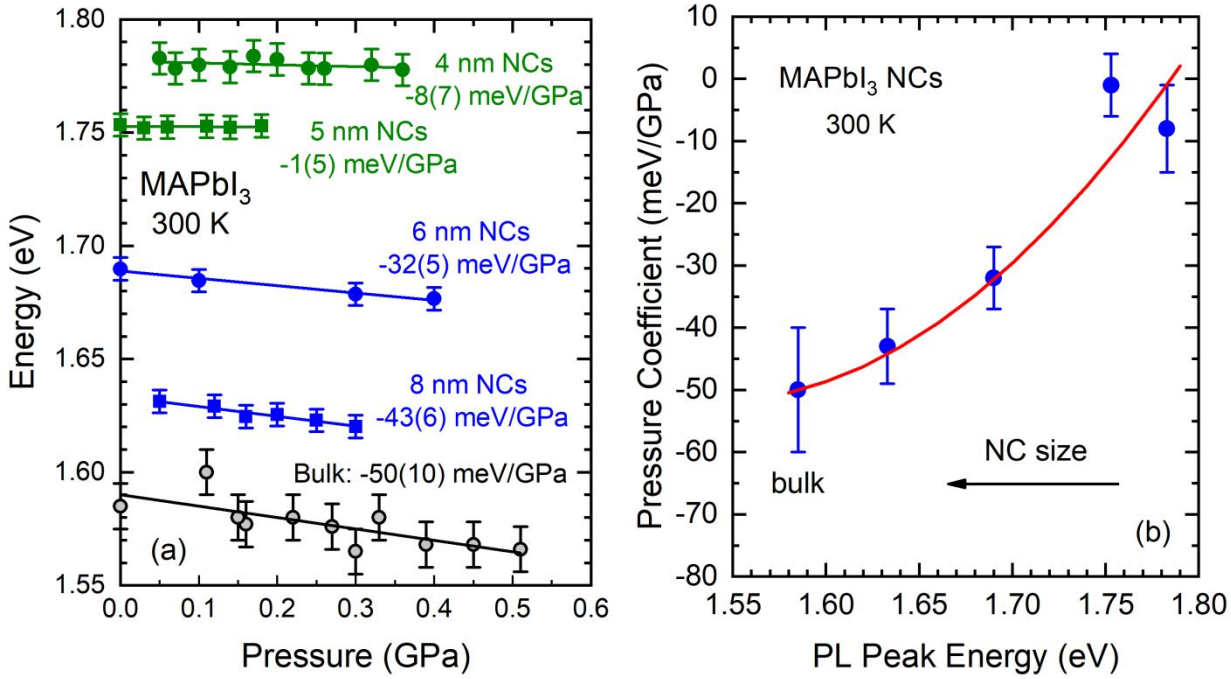

Figure 4: (a) Pressure dependence of PL peak energy for a $MAPbI_3$ bulk sample (black/grey dots) and several composite samples with nanocrystals of different size (blue and green symbols). The slopes of the linear regressions represented by the solid lines are indicated. (b) The pressure coefficients obtained from the slopes of the lines in (a) plotted as a function of the gap energies extrapolated to ambient pressure conditions from the linear fits in (a). The red curve is a fit to the data points using an empirical quadratic function.

At this point, we have all we need to determine the relative contributions from thermal expansion and electron-phonon coupling to the temperature-induced renormalization of the gap for the five samples we have presented in Fig. 3, listed in Table I. The first column in Table I corresponds to the values of gap energy at ambient conditions $E_{g,300\,K}$, obtained directly from the data points in Fig. 3. The second column lists the values of the linear pressure coefficients computed at the respective $E_{g,300\,K}$ energies by interpolation using the red curve in the graph of Fig. 4b. The TE contribution (third column in Table I) is thus obtained by evaluating Eq. (2), using the previously computed pressure coefficients, a volumetric thermal expansion coefficient[48] α_v=1.27x10^{-4} K^{-1} and a bulk modulus[44] B_0=16.5 GPa, both from the literature. Here we assume that both TE coefficient and bulk modulus do not depend on NC size, as supported by the experimental evidence available for metal halide perovskites.[49] The fourth column of Table I

contains the temperature coefficients of the gap for the tetragonal phase of the five $MAPbI_3$ samples directly obtained from the slopes of the linear regressions drawn in Fig. 3 (cyan curves). Using Eq. (1), the electron-phonon contribution is calculated by subtracting the TE term from the temperature slopes. The last column of Table I finally represents the weight of each contribution (TE and EP) to the total gap renormalization, expressed in percentage of the total. Strikingly, the weight of the electron-phonon coupling increases from 50% as in bulk to about 75% for nanocrystals of a few nanometers in diameter.

$MAPbI_3$	$E_{g,300\,K}$ (eV)	dE_g/dP (meV/GPa)	TE (meV/K)	dE_g/dT (meV/K)	EP (meV/K)	TE/EP (%)
Bulk	1.589(5)	-50(10)	0.11(3)	0.22(1)	0.11(4)	50/50
Thin film	1.605(5)	-49(10)	0.10(3)	0.20(2)	0.10(5)	50/50
8 nm NCs	1.677(5)	-35(6)	0.07(2)	0.21(2)	0.14(4)	33/67
5 nm NCs	1.739(5)	-18(5)	0.04(2)	0.19(3)	0.15(5)	21/79
4 nm NCs	1.766(5)	-8(5)	0.02(2)	0.07(5)	0.05(7)	28/72

Table I: Estimation of the contributions from thermal expansion (TE) and electron-phonon interaction (EP) to the renormalization of the gap energy for the room-temperature tetragonal phase of the $MAPbI_3$ NCs, the thin film and the bulk form. $E_{g,300\,K}$ corresponds to the gap energy E_g at room temperature, dE_g/dP is the measured gap pressure coefficient and TE represents the thermal expansion contribution calculated using Eq. (2). The electron-phonon (EP) contribution is computed by subtracting the TE term from the measured temperature slope dE_g/dT. The last column represents the weight of each contribution to the total gap renormalization, expressed in percentage of the total. Numbers in parentheses represent the error bars.

A comparison between the estimated NC sizes with the extension of the exciton Bohr radius in $MAPbI_3$, which is approximately 3 nm,[50] sheds light on the observed size dependence of the EP term. Excitons in the smaller size NCs would exhibit strong confinement effects of

their wave function, ultimately leading to an enhanced overlap with the NC phonons, i.e., a stronger electron-phonon coupling. It is precisely for those nanocrystals whose radii are smaller than the exciton R_B for which we observe an enhancement of the EP contribution, in good agreement with this hypothesis. Hence we can argue that the variation of the wave function overlap between exciton and phonons is the reason that leads to appreciable changes in the temperature-induced renormalization of the gap energy. We emphasize that the conclusions about the enhancement of the electron-phonon interaction at the nanoscale as a result of quantum confinement effects is model independent. The EP term was simply obtained by subtracting two experimentally determined quantities. This, in turn, leads to more accurate values for the electron-phonon interaction contribution to the temperature-induced gap renormalization, avoiding making any assumption about thermal expansion effects.

In conclusion, by combining PL measurements as a function of temperature and pressure, we were able to separate the different contributions from thermal expansion and electron-phonon interaction effects to the temperature-induced renormalization of the gap for $MAPbI_3$ nanocrystals, and compare them to the cases of thin films and single-crystalline bulk. A striking result of this work concerns the enhancement of the electron-phonon coupling term, whose relative weight increases from 50% in bulk up to 75% for NCs with effective radii below 3 nm. We argue that such enhancement is a consequence of the increased wave function overlap between electrons and phonons, due to strong quantum confinement effects on the NC excitons.

Acknowledgements

Funding for this work was provided by the Spanish "Ministerio de Ciencia, Innovación y Universidades (MCIU)" through Grants SEV-2015-0496 and CEX2019-000917-S, in the framework of the Spanish Severo Ochoa Centre of Excellence program, the AEI/ FEDER(UE) grants MAT2015-70850-P (HIBRI2), MAT2017-88584-R (MODO) and PGC2018-095411-B-100 (RAINBOW), and the FPI fellowships BES-2016-076913 (AFL) and BES-2015-072687 (AR). The Catalan agency AGAUR is also acknowledged for grant 2017-SGR-00488. The authors are also grateful to the National Network "Red Perovskitas" (MCIU funded) and the Center of Technological Research and Innovation of the University of Seville (CITIUS), where structural characterization was performed

Supporting Information

Experimental methods; sample preparation; structural characterization by TEM, X-ray diffraction and Raman scattering as a function of temperature; discussion on the excitonic character of the PL emission; nanocrystal size estimations using Brus formula; examples of the line shape fitting procedure using a Gaussian-Lorentzian cross-product function for the analysis of the temperature-dependent PL spectra; discussion on the temperature dependence of the FWHM and integrated PL intensities; discussion on potentially relevant effects at T<240 K.

REFERENCES

(1) Quan, L. N.; Rand, B. P.; Friend, R. H.; Mhaisalkar, S. G.; Lee, T.-L.; Sargent, E. H. Perovskites for Next-Generation Optical Sources. *Chem. Rev.* **2019**, 119, 7444-7477.

(2) Manser, J. S.; Christians, J. A.; Kamat, P. V. Intriguing Optoelectronic Properties of Metal Halide Perovskites. *Chem. Rev*. **2016**, 116, 12956-13008.

(3) Klingshirn, C. F. *Semiconductor Optics* **1997** (Springer, Berlin).

(4) Schmidt, L. C.; Pertegás, A.; González-Carrero, S.; Malinkiewicz, O.; Agouram, S.; Mínguez Espallargas, G.; Bolink, H. J.; Galian, R. E.; Pérez-Prieto, J. Nontemplate Synthesis of $CH_3NH_3PbBr_3$ Perovskite Nanoparticles. *J. Am. Chem. Soc.* **2014**, 136, 850-853.

(5) Protesescu, L.; Yakunin, S.; Bodnarchuk, M. I.; Krieg, F.; Caputo, R.; Hendon, C. H.; Yang, R. X.; Walsh, A.; Kovalenko, M. V. Nanocrystals of Cesium Lead Halide Perovskites ($CsPbX_3$, X = Cl, Br, and I): Novel Optoelectronic Materials Showing Bright Emission with Wide Color Gamut. *Nano Lett.* **2015**, 15, 3692-3696.

(6) Rubino, A.; Caliò, L.; García-Bennett, A.; Calvo, M. E.; Míguez, H. Mesoporous Matrices as Hosts for Metal Halide Perovskite Nanocrystals. *Adv. Optical Mater.* **2020**, 8, 1901868.

(7) Dirin, D. N.; Protesescu, L.; Trummer, D.; Kochetygov, I. V.; Yakunin, S.; Krumeich, F.; Stadie, N. P.; Kovalenko, M. V. Harnessing Defect-Tolerance at the Nanoscale: Highly Luminescent Lead Halide Perovskite Nanocrystals in Mesoporous Silica Matrixes. *Nano Lett.* **2016**, 16, 5866-5874.

(8) Shi, Z.-F.; Li, Y.; Li, S.; Ji, H.-F.; Lei, L.-Z.; Wu, D.; Xu, T.-T.; Xu, J.-M.; Tian, Y.-T.; Li, X.-J. Polarized Emission Effect Realized in CH3NH3PbI3 Perovskite Nanocrystals. J. Mater. Chem. C **2017**, 5, 8699-8706.

(9) Diroll, B. T.; Guo, P.; Schaller, R. D. Unique Optical Properties of Methylammonium Lead Iodide Nanocrystals Below the Bulk Tetragonal-Orthorhombic Phase Transition. *Nano Lett.* **2018**, 18, 846-852.

(10) Rubino, A.; Anaya, M.; Galisteo-López, J. F.; Rojas, T. C.; Calvo, M. E.; Míguez, H. Highly Efficient and Environmentally Stable Flexible Color Converters Based on Confined $CH_3NH_3PbBr_3$ Nanocrystals. *ACS Appl. Mater. Interfaces* **2018**, 10, 38334-38340.

(11) Woo, H. C.; Choi, J. W.; Shin, J.; Chin, S.-H.; Ann, M. H.; Lee, C.-L. Temperature-Dependent Photoluminescence of $CH_3NH_3PbBr_3$ Perovskite Quantum Dots and Bulk Counterparts. *J. Phys. Chem. Lett.* **2018**, 9, 4066-4074.

(12) Glinka, Y. D.; Cai, R.; Gao, X.; Wu, D.; Chen, R.; Sun, X. W. Structural Phase Transitions and Photoluminescence Mechanism in a Layer of 3D Hybrid Perovskite Nanocrystals. *AIP Adv.* **2020**, 10, 065028/1-19.

(13) Ijaz, P.; Imran, M.; Soares, M. M.; Tolentino, H. C. N.; Martín-García, B.; Giannini, C.; Moreels, I.; Manna, L.; Krahne, R. Composition-, Size-, and Surface Functionalization-Dependent Optical Properties of Lead Bromide Perovskite Nanocrystals. *J. Phys. Chem. Lett.* **2020**, 11, 2079-2085.

(14) Fang, H.-H.; Protesescu, L.; Balazs, D. M.; Adjokatse, S.; Kovalenko, M. V.; Loi, M. A. Exciton Recombination in Formamidinium Lead Triiodide: Nanocrystals versus Thin Films. *Small* **2017**, 13, 1700673/1-10.

(15) Fu, M.; Tamarat, P.; Trebbia, J. B.; Bodnarchuk, M. I.; Kovalenko, M. V.; Even, J.; Lounis, B. Unraveling Exciton-Phonon Coupling in Individual $FAPbI_3$ Nanocrystals Emitting Near-Infrared Single Photons. *Nature Commun.* **2018**, *9*, 3318-3327.

(16) Ghosh, S.; Shi, Q.; Pradhan, B.; Kumar, P.; Wang, Z.; Acharya, S.; Pal, S. K.; Pullerits, T.; Karki, K. J. Phonon Coupling with Excitons and Free Carriers in Formamidinium Lead Bromide Perovskite Nanocrystals. *J. Phys. Chem. Lett.* **2018**, *9*, 4245-4250.

(17) Pfingsten, O.; Klein, J.; Protesescu, L.; Bodnarchuk, M. I.; Kovalenko, M. V.; Bacher, G. Phonon Interaction and Phase Transition in Single Formamidinium Lead Bromide Quantum Dots. *Nano Lett.* **2018**, 18, 4440-4446.

(18) Saran, R.; Heuer-Jungemann, A.; Kanaras, A. G.; Curry, R. J. Giant Bandgap Renormalization and Exciton-Phonon Scattering in Perovskite Nanocrystals. *Adv. Optical Mater*. **2017**, 5, 1700231/1-9.

(19) Lee, S. M.; Moon, C. J.; Lim, H.; Lee, Y.; Choi, M. Y.; Bang, J. Temperature-Dependent Photoluminescence of Cesium Lead Halide Perovskite Quantum Dots: Splitting of the Photoluminescence Peaks of $CsPbBr_3$ and $CsPb(Br/I)_3$ Quantum Dots at Low Temperature. *J. Phys. Chem. C* **2017**, 121, 26054-26062.

(20) Liu, A.; Bonato, L. G.; Sessa, F.; Almeida, D. B.; Isele, E.; Nagamine, G.; Zagonel, L. F.; Nogueira, A. F.; Padilha, L. A.; Cundiff, S. T. Effect of Dimensionality on the Optical Absorption Properties of $CsPbI_3$ Perovskite Nanocrystals. *J. Chem. Phys.* **2019**, 151, 191103.

(21) Li, J.; Yuan, X.; Jing, P.; Li, J.; Wei, M.; Hua, J.; Zhao, J.; Tian, L. Temperature-Dependent Photoluminescence of Inorganic Perovskite Nanocrystal Films. *RSC Adv.* **2016**, 6, 78311-78316.

(22) Iaru, C. M.; Geuchies, J. J.; Koenraad, P. M.; Vanmaekelbergh, D.; Silov, A. Y. Strong Carrier−Phonon Coupling in Lead Halide Perovskite Nanocrystals. *ACS Nano* **2017**, 11, 11024-11030.

(23) Fu, M.; Tamarat, P.; Huang, H.; Even, J.; Rogach, A. L.; Lounis, B. Neutral and Charged Exciton Fine Structure in Single Lead Halide Perovskite Nanocrystals Revealed by Magneto-Optical Spectroscopy. *Nano Lett.* **2017**, 17, 2895-2901.

(24) Beimborn II, J. C.; Walther, L. R.; Wilson, K. D.; Weber, J. M. Size-Dependent Pressure-Response of the Photoluminescence of $CsPbBr_3$ Nanocrystals. *J. Phys. Chem. Lett.* **2020**, 11, 1975-1980.

(25) Lautenschlager, P.; Allen, P. B.; Cardona, M. Temperature Dependence of Band Gaps in Si and Ge. *Phys. Rev. B* **1985**, 31, 2163-2171.

(26) Gopalan, S.; Lautenschlager, P.; Cardona, M. Temperature Dependence of the Shifts and Broadenings of the Critical Points in GaAs. *Phys. Rev. B* **1987**, 35, 5577-5584.

(27) Cardona, M. Electron-Phonon Interaction in Tetrahedral Semiconductors. *Solid State Commun.* **2005**, 133, 3-18.

(28) Lautenschlager, P.; Garriga, M.; Logothetidis, S.; Cardona, M. Interband Critical Points of GaAs and their Temperature Dependence. *Phys. Rev. B* **1987**, 35, 9174-9189.

(

29) Foley, B. J.; Marlowe, D. L.; Sun, K.; Saidi, W. A.; Scudiero, L.; Gupta, M. C.; Choi, J. J. Temperature Dependent Energy Levels of Methylammonium Lead Iodide Perovskite. *Appl. Phys. Lett.* **2015**, 106, 243904/1-5.

(30) Milot, R. L.; Eperon, G. E.; Snaith, H. J.; Johnston, M. B.; Herz, L. M. Temperature-Dependent Charge-Carrier Dynamics in $CH_3NH_3PbI_3$ Perovskite Thin Films. *Adv. Funct. Mater.* **2015**, 25, 6218-6227.

(31) Dar, M. I.; Jacopin, G.; Meloni, S.; Mattoni, A.; Arora, N.; Boziki, A.; Zakeeruddin, S. M.; Rothlisberger, U.; Grätzel, M. Origin of Unsusual Gap Shift and Dual Emission in Organic-Inorganic Lead Halide Perovskites. *Sci. Adv.* **2016**, 2, e1601156/1-9.

(32) Wright, A. D.; Verdi, C.; Milot, R. L.; Eperon, G. E.; Pérez-Osorio, M. A.; Snaith, H. J.; Giustino, F.; Johnston, M. B.; Herz, L. M. Electron-Phonon Coupling in Hybrid Lead Halide Perovskites. *Nature Commun.* **2016**, 7, 11755/1-9.

(33) Kim, H.; Hunger, J.; Cánovas, E.; Karakus, M.; Mics, Z.; Grechko, M.; Turchinovich, D.; Parekh, S. H.; Bonn, M. Direct Observation of Mode-Specific Phonon-Band Gap Coupling in Methylammonium Lead Halide Perovskites. *Nature Commun.* **2017**, 8, 687/1-9.

(34) Francisco López, A.; Charles, B.; Weber, O. J.; Alonso, M. I.; Garriga, M.; Campoy-Quiles, M.; Weller, M. T.; Goñi, A. R. Equal Footing of Thermal Expansion and Electron-Phonon Interaction in the Temperature Dependence of Lead Halide Perovskite Band Gaps. *J. Phys. Chem. Lett.* **2019**, 10, 2971-2977.

(35) Saidi, W. A.; Poncé, S.; Monserrat, B. Temperature Dependence of the Energy Levels of Methylammonium Lead Iodide Perovskite from First-Principles. *J. Phys. Chem. Lett.* **2016**, 7, 5247-5252.

(36) Saidi, W. A.; Kachmar, A. Effects of Electron-Phonon Coupling on Electronic Properties of Methylammonium Lead Iodide Perovskites. *J. Phys. Chem. Lett.* **2018**, 9, 7090-7097.

(37) Francisco López, A.; Charles, B.; Weber, O. J.; Alonso, M. I.; Garriga, M.; Campoy-Quiles, M.; Weller, M. T.; Goñi, A. R. Phase Diagram of Methylammonium/Formamidinium Lead Iodide Perovskite Solid Solutions from Temperature Dependent Photoluminescence and Raman Spectroscopies. *J. Phys. Chem. C* **2019**, 124, 3448-3458.

(38) Francisco López, A.; Charles, B.; Weber, O. J.; Alonso, M. I.; Garriga, M.; Campoy-Quiles, M.; Weller, M. T.; Goñi, A. R. Pressure-Induced Locking of Methylammonium Cations Versus Amorphization in Hybrid Lead Iodide Perovskites. *J. Phys. Chem. C* **2018**, 122, 22073-22082.

(39) Brus, L. E. Electron-Electron and Electron-Hole Interactions in Small Semiconductor Crystallites: The Size Dependence of the Lowest Excited Electronic State. *J. Chem. Phys.* **1984**, 80, 4403-4409.

(40) Weller, M. T.; Weber, O. J.; Henry, P. F.; Di Pumpo, A. M.; Hansen, T. C. Complete Structure and Cation Orientation in the Perovskite Photovoltaic Methylammonium Lead Iodide Between 100 and 352 K. *Chem. Commun.* **2015**, 51, 4180-4183.

(41) Miyata, A.; Mitioglu, A.; Plochocka, P.; Portugall, O.; Wang, J. T.-W.; Stranks, S. D.; Snaith, H. J.; Nicholas, R. J. Direct Measurement of the Exciton Binding Energy and Effective Masses for Charge Carriers in Organic-Inorganic Tri-Halide Perovskites. *Nature Phys.* **2015**, 11, 582-587.

(42) Phuong, L. Q.; Nakaike, Y.; Wakamiya, A.; Kanemitsu, Y. Free Excitons and Exciton-Phonon Coupling in $CH_3NH_3PbI_3$ Single Crystals Revealed by Photocurrent and Photoluminescence Measurements at Low Temperatures. *J. Phys. Chem. Lett.* **2016**, 7, 4905-4910.

(43) Ghosh, D.; Aziz, A.; Dawson, J. A.; Walker, A. B.; Islam, M. S. Putting the Squeeze on Lead Iodide Perovskites: Pressure-Induced Effects to Tune Their Structural and Optoelectronic Behavior. *Chem. Mater.* **2019**, 31, 4063-4071.

(44) Szafrański, M.; Katrusiak, A. Mechanism of Pressure-Induced Phase Transitions, Amorphization, and Absorption-Edge Shift in Photovoltaic Methylammonium Lead Iodide. *J. Phys. Chem. Lett.***2016**, 7, 3458-3466.

(45) Hannah, D. C.; Yang, J.; Podsiadlo, P.; Chan, M. K. Y.; Demortière, A.; Gosztola, D. J.; Prakapenka, V. B.; Schatz, G. C.; Kortshagen, U.; Schaller, R. D. On the Origin of Photoluminescence in Silicon Nanocrystals: Pressure-Dependent Structural and Optical Studies. *Nano Lett.* **2012**, *12*, 4200-4205.

(46) Goñi, A. R.; Muniz, L. R.; Reparaz, J. S.; Alonso, M. I.; Garriga, M.; Lopeandia, A. F.; Rodríguez-Viejo, J.; Arbiol, J.; Rurali, R. Using High Pressure to Unravel the Mechanism of Visible Emission in Amorphous Si/SiOx Nanoparticles. *Phys. Rev. B* **2014**, 89, 045428/1-13.

(47) Lin, Y.-C.; Chou, W.-C.; Susha, A. S.; Kershaw, S. V.; Rogach, A. L. Photoluminescence and Time-Resolved Carrier Dynamics in Thiol Capped CdTe Nanocrystals under High Pressure. *Nanoscale* **2013**, *5*, 3400-3405.

(48) Whitfield, P. S.; Herron, N.; Guise, W. E.; Page, K.; Cheng, Y. Q.; Milas, I.; Crawford, M. K. Structures, Phase Transitions and Tricritical Behavior of the Hybrid Perovskite Methyl Ammonium Lead Iodide. *Sci. Rep.* **2016**, 6, 35685/1-15 and the corrigendum in idem, *Sci. Rep.* **2017**, 7, 42831.

(49) Li, M.; Liu, T.; Wang, Y.; Yang, W.; Lü, X. Pressure Responses of Halide Perovskites with Various Compositions, Dimensionalities, and Morphologies. *Matter Radiat. Extremes* **2020**, 5, 018201/1-15.

(50) Tanaka, K.; Takahashi, T.; Ban, T.; Kondo, T.; Uchida, K.; Miura, N. Comparative study on the excitons in lead-halide-based perovskite-type crystals $CH_3NH_3PbBr_3$ $CH_3NH_3PbI_3$. *Solid State Commun.* **2003**, 127, 619−623.